Journal of Sedimentary Research

Journal of Sedimentary Research, 2008, v. 78, 579–593
Research Article
DOI: 10.2110/jsr.2008.059

VALLEYS THAT NEVER WERE: TIME SURFACES VERSUS STRATIGRAPHIC SURFACES

NIKKI STRONG AND CHRIS PAOLA
National Center for Earth-surface Dynamics (NCED), Department of Geology and Geophysics, University of Minnesota, St. Anthony Falls Laboratory, 2 at Third Avenue SE, Minneapolis, Minnesota 55414, U.S.A.

ABSTRACT: **Using experimental data, we show how erosional unconformities (sequence boundaries) form and evolve in response to changes in global sea level (eustasy), given passive margin style subsidence and constant conditions of supply of sediment and water. We distinguish between two types of erosional unconformities; broad planar erosional surfaces that form during relatively slow sea-level fall, and incised-valleys that form during relatively rapid sea-level fall. We find that both types of unconformities evolve continuously throughout both sea-level fall and rise, producing erosional surfaces that are highly diachronous and amalgamated. We focus mostly on the role of change in relative sea level (RSL) on the formation of incised valleys and their preservation in the stratigraphic record. We find that there is an ongoing interplay of erosion and deposition that continuously redefines the shape of an incised valley, such that valleys both narrow and widen as they deepen during RSL fall and then continue to widen and fill during RSL rise. Due to this dynamic reshaping, what is preserved in stratigraphy may resemble a valley in shape, but its geomorphic form likely never existed in the fluvial landscape. We also find that these erosional valleys tend to be most diachronous along lateral margins of valley fill in proximal areas of the basin and become somewhat younger on average landward along their axial parts. Overall, the basal erosional unconformity forms over most of the duration of the sea-level cycle, does not represent a topographic surface, and is therefore not a time line. Finally, because valleys form through a continuous process of channel incision, backfill, and channel migration (avulsion) during RSL fall, earlier fluvial fills can lie on top of the extended erosional surface, which overrides successively younger delta fronts as it develops. Thus, although locally the deposits above the unconformity are always younger than those below it, the unconformity spans so much time that some of the deposits above it end up being older than some of the deposits below it. The net result is that there are numerous, though relatively small-scale, deviations from one of the frequently quoted fundamental characteristics of a sequence boundary, which is that rocks above it be everywhere younger than rocks below it.**

INTRODUCTION

A good deal has been written on the geology of incised valleys, and what they can tell us about the geological history of an area. We look to incised valleys for evidence of sea-level change, episodic tectonic uplift, subsidence, and climate change (Kraus and Middleton 1987; Bromely 1991; Lopez-Gomez and Arche 1993; Ashley and Sheridan 1994; Blum and Törnqvist 2000). Erosional unconformities associated with incised valleys are typically large-scale, easily recognizable surfaces and therefore are considered useful tools for correlating chronostratigraphic units, e.g., in seismic section, well logs, and outcrop (e.g., Van Wagoner et al. 1990). In addition, incised valleys are often associated with large-scale sediment-bypass zones that feed downdip into large sandy deltas. Therefore there is also a keen interest in characterizing the geometry and fill of these valleys in stratigraphy, to better predict downstream reservoir potential (Dalrymple 2001; Van Heijst and Postma 2001).

Incised valleys preserved in the stratigraphic record are valley-form erosional surfaces that resemble incisional valleys observed on the Earth's surface today. So it is natural to think that the erosional surfaces we see preserved stratigraphically represent buried valleys, i.e., buried topographic surfaces. The purpose of this paper is to explore this assumption via physical experiments in which we can observe and measure valley formation on the surface as well as the resultant deposit. We distinguish between *topographic valleys*, valleys defined by surface topography at some instant in time, and *stratigraphic valleys*, which are preserved valley-form erosional surfaces in the stratigraphic record. Both are produced by incision, and so either could be termed an "incised valley." The most common allogenic (caused by external factors) cause of incision is a fall in relative sea level (or lake or reservoir level), but an incised valley can also be created by tectonic tilting, faulting, or changes in relative supplies of water and sediment. Stratigraphic incised-valley surfaces play an important role in sequence stratigraphy in that they are a common type of sequence boundary (Van Wagoner et al. 1988; Posamentier and Allen 1999). There has been significant debate about the extent to which such sequence boundaries are time-transgressive (Blum and Price 1998; Catuneanu et al. 1998; Van Heijst et al. 2001; Törnqvist et al. 2003). The degree of diachrony of an erosional surface bears directly on the relation between the topographic surface and the surface as preserved stratigraphically. Any preserved surface that represents a single instant in time, i.e., that is buried without modification, is not time-transgressive, and by definition is equivalent to a topographic surface. If a topographic surface persists over some time interval, then it could be said to be time transgressive (in terms of when it formed), but if it is buried intact it still serves as a time marker, except that in this case it is a finite interval. More commonly, the topographic surface changes in time, and the associated stratal boundaries are composite surfaces that do not reflect any instantaneous topographic surface and are time transgressive. The

 1527-1404/08/078-579/$03.00

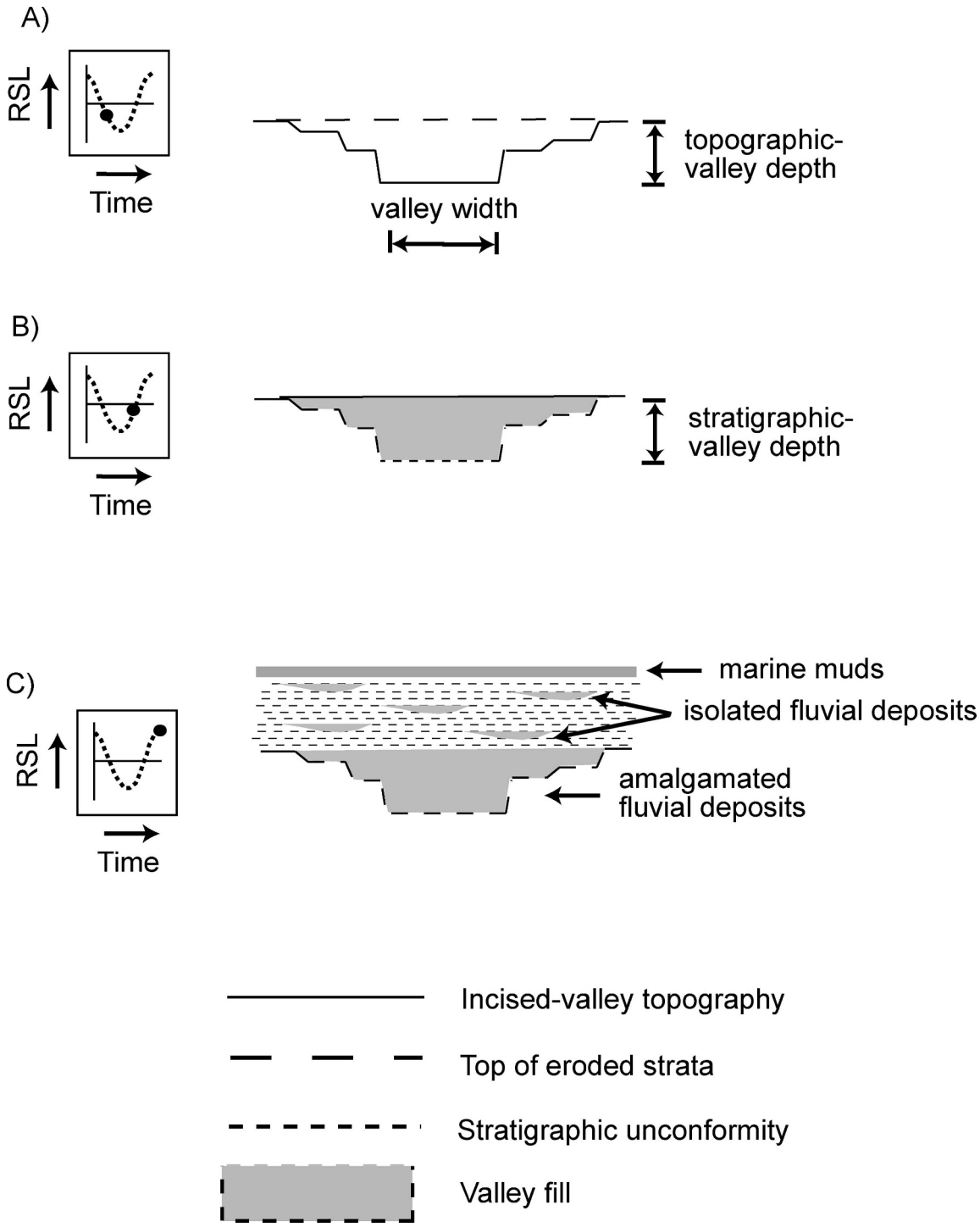

FIG. 1.—Shanley and McCabe's (1993, 1994, 1998) model for development of depositional sequences in mixed fluvial–coastal–marine strata of the Cretaceous Western Interior basin of the USA, in response to relative sea-level (RSL) change, illustrating the concept of **A)** incision and sediment bypass during base-level fall that is common to many sequence stratigraphic models, followed by valley filling, **B)** first with amalgamated fluvial deposits, then **C)** estuarine deposits, capped by marine muds.

bounding surfaces commonly produced by migrating bedforms (Brookfield 1977; Rubin 1987) are a good example of this: over bedform-migration time scales they are time transgressive, and morphologically they generally do not resemble the bedforms that produced them.

If the preserved stratigraphic surface "looks like" the topographic feature thought to have produced it, the relationship between the two is unclear and bears investigation both in terms of topographic versus stratigraphic morphology, and the closely related question of diachrony of the preserved surface. Sheets and Paola (2008) found, for instance, that preserved river channels are composite surfaces that, while generally similar to channels in form, are morphologically different from any of the instantaneous topographic channels that produced them.

A simple model for incised-valley evolution is shown in the idealized sketches in Figure 1, after Shanley and McCabe (1993, 1994, 1998). The

valley incises during falling stages of relative sea level, and fluvial deposits are deposited during the late stages of sea-level fall and the early rise. Estuarine deposits are deposited later during rising relative sea level. Once the valley is filled, it is then capped by marine mud. The key point is that first, the valley is created by incision, during relative base-level fall, and then it is filled by deposition. Once formed, the erosional surface defining the shape of the valley remains unchanged—the valley "container" passively fills up with sediment.

If the above scenario were what actually happens in nature, the topographic valley at the time of maximum excavation would be identical to the preserved stratigraphic valley. We show here that instead, processes associated with valley incision and filling control the relation between topographic and final preserved (stratigraphic) valley shape. Many workers have pointed out that the processes by which valleys fill via episodes of erosion and deposition, including those that form terraces, are more complex than represented by the simple model above (Schumm 1977; Catuneanu et al. 1998; Blum and Törnqvist 2000; Weissmann et al. 2002; Ethridge et al. 2005). In interpreting this complexity, it is easy to fall into the trap of thinking that every effect has a single cause, e.g., complexity is driven by discrete external (allogenic) forcing mechanisms.

We (Strong and Paola 2006) used data from the same experiment to explore how autogenic fluvial processes can produce complex landscapes and stratigraphy that do not necessarily reflect allogenic forcing on the system, i.e., discrete changes in eustasy, tectonics, or climate. For example, we illustrated how, during falling relative sea level and valley incision, episodes of valley narrowing can produce a complex step-like morphology of unpaired autogenic terraces, despite smooth, continuous sea-level fall. Here we show how the interplay of erosion and deposition continually redefines the shape of an incised valley not only during valley incision but also during and after valley filling. We demonstrate that, due to this dynamic reshaping, the shape of a valley preserved in stratigraphy may bear little resemblance to any incised valley that ever existed in the landscape. We then develop a dimensionless time scale to quantify the extent to which this energetic reshaping causes the walls and floor of the incised valley to be highly diachronous in both strike and dip directions.

As noted by Strong and Paola (2006), the advantage of using experiments for this kind of analysis is that the experiment allows us to observe the complete process of valley incision, filling, and preservation as stratigraphy. Here we also take advantage of the fact that experimental data can give us a quantitative measure of valley evolution with high temporal and spatial resolution. We use this data to age-date the entire erosional unconformity associated with the incised valley.

EXPERIMENTAL METHODS

The experimental data presented in this paper come from an experiment conducted in the Experimental EarthScape (XES) facility, St. Anthony Falls Laboratory, University of Minnesota, Twin Cities (Heller et al. 2001; Paola et al. 2001; Sheets et al. 2002; Strong et al. 2005; Kim et al. 2006; Strong 2006; Strong and Paola 2006) This study was designed to examine morphodynamic and stratigraphic response to both isolated and superimposed slow and rapid eustatic cycles, in a siliciclastic fluvial-deltaic system subject to steady, non-uniform passive-margin-style subsidence and constant supply of water and sediment. The evolution of the surface topography, flow pattern, and stratigraphy in the experiment is entirely the result of the internal organization of the sediment system in response to the externally imposed conditions discussed in this section.

XES Basin

The XES facility is a large (13 m $\times$ 6 m $\times$ 1.3 m) experimental basin with a programmable subsiding floor. Water discharge and sediment discharge into the basin, as well as base level (the experimental equivalent of eustasy), are also fully controllable. This run of the XES basin (XES 02) used one fourth of the total width of the XES basin (3 m of the available 12 m), and modeled basin filling by a braided river system prograding into a standing body of water in a manner similar to that of a Gilbert-type braided fluvial fan delta as defined by Nemec and Steel (1984). Since the objective of this run was to isolate and identify the effects of changes in sea level on basin geomorphology and stratigraphy, sediment supply and water supply were held constant during the run as well as rates and geometry of subsidence. A schematic diagram of the experimental basin in dip section (parallel to the mean flow direction) and plan view is shown in Figure 2A.

Eustatic Sea-Level Cycles

In XES 02, global sea level (GSL) is the elevation of the surface of the standing body of water at the distal (downstream) end of the experimental basin measured relative to a stationary datum, the upper rim of the experimental basin (Fig. 2A). Fluctuations in GSL in the XES basin represent natural global sea-level (eustatic) changes. The GSL curve for the run is shown in Figure 2B.

As shown in Figure 2B, the experiment was divided into two stages: Stage I, with isolated slow and rapid sea-level cycles, was intended as a study of basic geomorphic and stratigraphic response as a function of cycle period, and Stage II, with superimposed slow and rapid GSL cycles, was intended to investigate the nonlinear interaction between two cycle periods, and thereby provide insight on the natural case, where eustatic cycles of multiple periods are superimposed.

The slow cycle period was designed to be longer, and the rapid cycle shorter, than the theoretical "equilibrium time" of the basin (Paola et al. 1992), where equilibrium time is the natural response time of a basin to imposed change and is calculated as a function of basin dimensions, as well as supply of sediment and water. For example, during a slow sea-level change, a basin theoretically is able to maintain a state of quasi-equilibrium, such that deposition and erosion are uniform across the width of the basin and transient surface response is averaged out. In contrast, during a rapid sea-level change a disequilibrium response, principally erosion during sea-level fall, produces valley incision. The ratio of the slow-cycle period to the rapid-cycle period, 6:1, was chosen to be comparable to the frequency ratio of long- and intermediate-period Milankovitch cycles.

This experiment was also designed so that the net GSL fall and GSL rise would be substantially larger than the maximum autogenic scour depth, estimated to be about 50 mm from previous experiments (Sheets et al. 2002), so that the stratigraphic signature of these two mechanisms of erosion could be distinguished in the stratigraphy. Furthermore, it was important that the net GSL fall and rise should be sufficiently small so that at the extremes of the superimposed cycles the shoreline would not be driven too far downstream during fall or upstream during rise. This was accomplished by using a 2D geometric model to estimate extremes in shoreline position for different combinations of sediment discharge into the basin and magnitudes of GSL change (see Kim et al. 2006) for further discussion on the 2D geometric model). Finally, it was important that the GSL cycle lengths give a clear separation of rapid and slow periods, without superimposing so many rapid cycles that their individual deposits would be hard to distinguish. Thus, the magnitude of GSL variation for both cycle frequencies was set at 110 mm, with a combined maximum GSL variation of 220 mm for the superimposed cycles.

Relative Sea Level

Relative sea level (RSL) enters stratigraphic dynamics mainly via its time rate of change, equal to the sum of the rates of change in GSL and basement elevation. Changes in basement elevation are typically attributed to tectonic uplift and subsidence, but they can also be caused

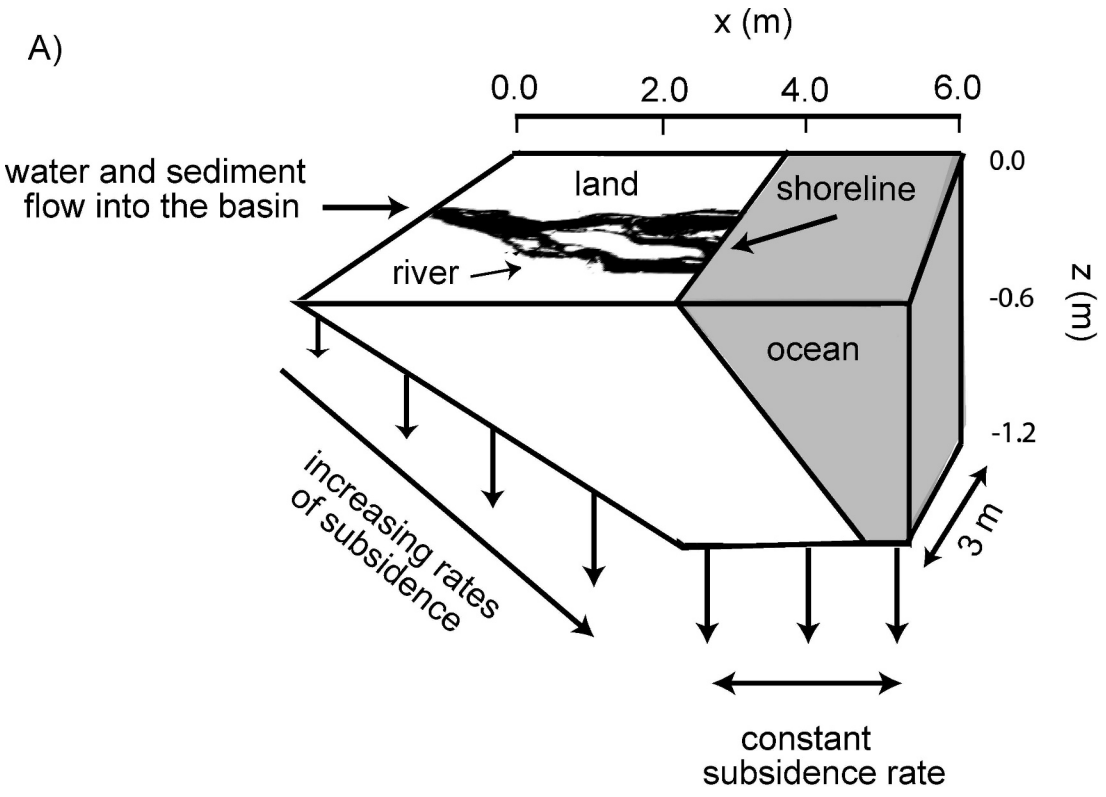
A)
x (m)
0.0
2.0
4.0
6.0
water and sediment
flow into the basin
land
shoreline
river
ocean
0.0
-0.6
-1.2
z (m)
increasing rates
of subsidence
3 m
constant
subsidence rate

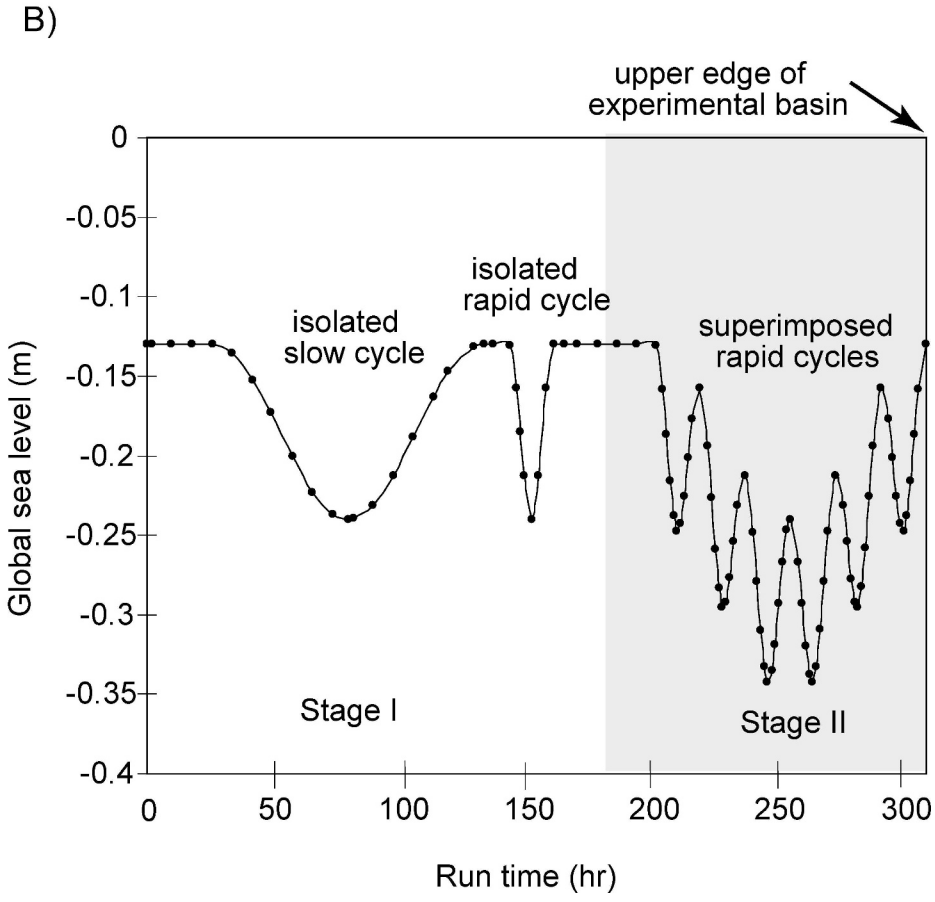
B)
upper edge of
experimental basin
0
-0.05
-0.1
-0.15
-0.2
-0.25
-0.3
-0.35
-0.4
Global sea level (m)
isolated
slow cycle
isolated
rapid cycle
superimposed
rapid cycles
Stage I
Stage II
0
50
100
150
200
250
300
Run time (hr)

by other processes, for example local small-scale faulting or sediment compaction. Since tectonic uplift and subsidence rates in nature tend to be laterally variable, the value of RSL(x, y, t) is a function of time and also on location in the basin. (In contrast, GSL(t) depends only on time.) The time rate of change in RSL(x, y, t) is given by

$$\frac{\partial RSL(x, y, t)}{\partial t} = \frac{dGSL(t)}{dt} + \sigma(x, y, t) \quad (1)$$

where GSL(t) refers to global sea level, $\sigma(x, y, t)$ refers to the time rate of change in the elevation of the surface of the Earth's crust, x and y refer to the depositional strike and dip coordinates respectively, and t is time. As we later demonstrate, while the value of RSL mainly controls valley depth, it is this time rate of change in RSL that controls valley width.

Subsidence

Subsidence rate $\sigma(x)$ in the XES 02 experiment was set to mimic a passive-margin spatial pattern and did not vary in the transverse direction or in time. The spatial pattern for local subsidence rate, $\sigma(x)$, is given by

$$\begin{aligned} \sigma(x) &= \frac{x}{L}\sigma_0 \; 0 \le x \le L \\ &= \sigma_0 \; x \ge L \end{aligned} \quad (2)$$

where σ_0 is local subsidence rate ($L\ T^{-1}$) at $x = L$ and is equal to 3.71 mm hr^{-1}. Here L refers to the distance from $x = 0$ to the change from increasing to constant subsidence rate at $x = 4000$ mm (Fig. 2A).

Supply of Sediment and Water

Sediment supply and water supply were held constant during the run. The total sediment discharge, 0.303 liters per minute, was set to 60% of the rate at which accommodation space (volume) was created. During the experiment a mix of water and sediment was fed into the experimental basin via a point source at its upstream end. This flowed into the basin, forming a braided fluvial fan delta whose shoreline migrated in response to varying base level (Fig. 2B). The sediment mixture consisted of 27% by volume crushed anthracite coal (100–700 μm), 63% by volume white quartz sand (120 μm), and 10% by volume kaolinite silica flour. To this mix 1.5% by weight titanium dioxide and 0.03% by weight PYLAM FDC Blue #1 dye (both in powder form) were added in order to increase visibility of surface flow in overhead photographs and videos. Coal and sand served as experimental proxies for fine- and coarse-grained sediment, respectively, with coal serving as the fine-grained proxy due to its lower density (1.4 g cm^{-3}), and thus a greater mobility relative to the quartz sand (2.65 g cm^{-3}). Also, in addition to the above sediment mix, 120 μm colored quartz sand was sprinkled onto the surface of the deposit at specified times during the run. Those colored sand horizons that remained preserved in the experimental deposit served as chronostratigraphic markers that proved to be invaluable in matching deposit features with recorded surface images and topographic and bathymetric scans.

We used a water discharge of 25 liters per minute and a sediment discharge of 0.303 liters per minute, for a sediment/water ratio of 0.01212. This gave us an equilibrium fluvial slope of 0.035 (comparable to the equilibrium slopes in XES Run 99 (Sheets et al. 2002; Strong et al. 2005).

DATA COLELCTION AND ANALYSIS

Surface Processes

The fluvial system was photographed with a digital video camera every two seconds while the system was running. In addition, a second video camera with a zoom lens was used to record specific events in greater detail, and to allow estimation of flow velocities by tracking bubbles on the water surface. Finally, the experimental surface was photographed with a high-resolution still camera every thirty minutes throughout the experiment, and every 15 minutes during the isolated rapid cycle.

Subaerial and Subaqueous Topography

Data on topographic elevation for the entire XES basin surface were collected at intervals ranging from 1.5 hr to 8 hr, depending on the phase of the experiment. A laser-sheet system was used to record the elevations of the subaerial part of the surface, and a 500 kHz sonar transducer was used to record the elevations of the submarine part of the surface. These instruments measured the elevations to a precision of 0.1 mm for subaerial elevations and 1 mm for subaqueous elevations. Elevations were collected every 10 mm across strike, with the laser scans spaced every 10 mm down dip and the sonar scans spaced every 50 mm down dip (Fig. 3A). A short video of the laser and sonar scanning system is available as supplementary material from the JSR data archive (see Acknowledgments section for URL).

Reconstructed Stratigraphy

Stratigraphic cross sections, in strike and dip section (Fig. 3B), were reconstructed by stacking in chronological order the laser and sonar elevation surfaces of the experimental deposit. The stacking is done by first migrating each surface to account for subsidence and then clipping it to account for erosion, as shown in Figure 3C.

Experimental Stratigraphy

The resultant experimental deposit was sectioned in strike section (cross-stream direction) for half the width of the basin and in dip section (streamwise direction) for the other half of the basin, providing a series of parallel faces spaced 10 mm apart in strike section and approximately 50 mm apart in dip section. These faces were imaged digitally and peels were taken periodically (Fig. 4).

EXPERIMENTAL OBSERVATIONS

As mentioned previously, by holding supply of water and sediment constant as well as subsidence rate, we intended to isolate the effects of GSL change on landscape evolution and alluvial stratigraphy, given a passive-margin-type subsidence pattern. We focus our discussion mostly on the role of GSL change on the formation of incised-valleys and their preservation in the stratigraphic record. We also restrict this discussion to subaerial (alluvial plain) incision, even though minor offshore subaqueous incision did occur as indicated in the topographic scans by slump scars and gullies on the experimental basin shelf slope. Images of the experimental basin shelf slope are available as supplementary material from the JSR data archive (see Acknowledgments section).

←

FIG. 2.— **A)** Schematic diagram of the experimental basin, the Experimental EarthScape (XES) facility at the National Center for Earth-surface Dynamics at St. Anthony Falls at the University of Minnesota, **B)** XES Run 02 global sea-level (GSL) curve. Dots on the curve indicate when topographic and bathymetric scans were taken during the experiment.

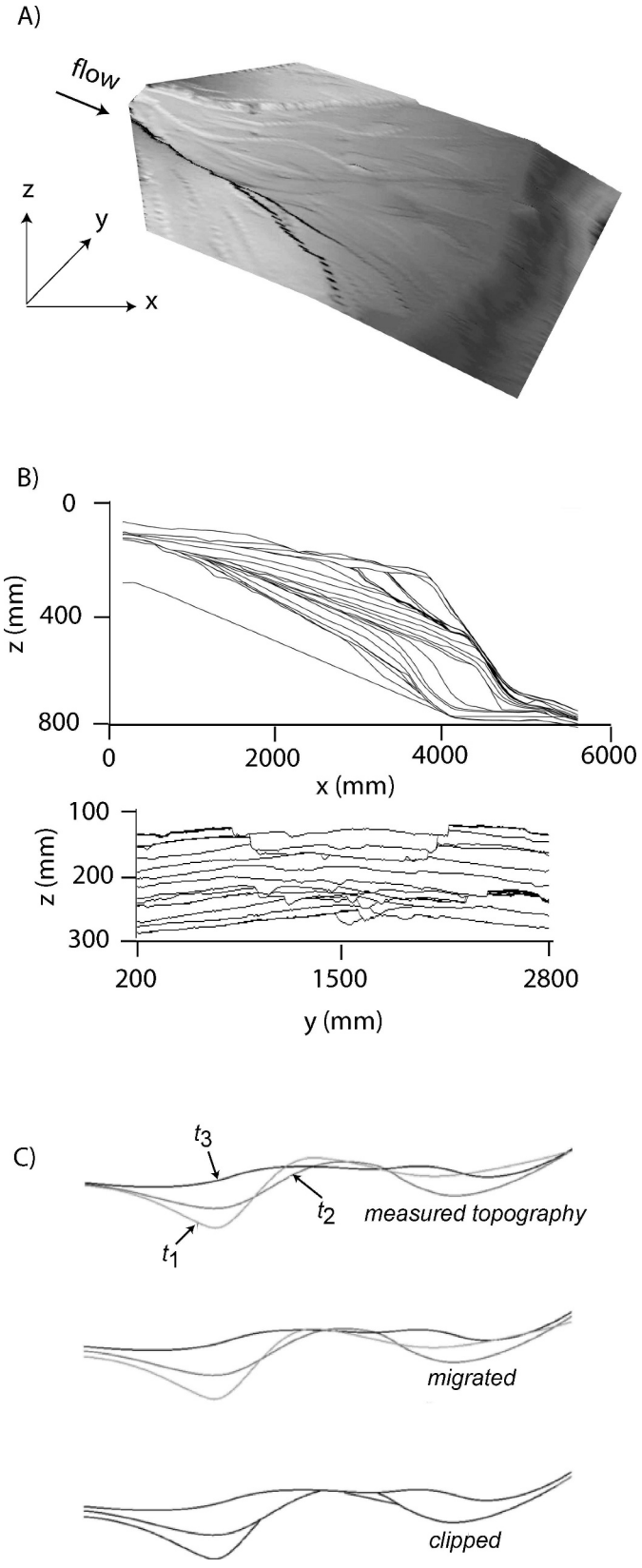

FIG. 3.—**A)** Topographic surface of the experiment at the end of the isolated GSL fall, reconstructed from the topographic and bathymetric scans, **B)** reconstructed stratigraphy from the topographic and bathymetric scans in dip (top figure) and strike (bottom figure) section, **C)** construction of the experimental reconstructed stratigraphy, illustrating first, the superposition of measured topographic profiles for scan times t_1, t_2, and t_3, second, the same topographic profiles, except migrated to account for tectonic subsidence, and third the migrated topographic profiles clipped to account for subsequent erosion. These migrated and clipped topographic profiles represent what we expect to see preserved as stratigraphy in the experimental basin.

Topographic-Valley Depth

During the isolated slow GSL fall, incision began at the upstream-most part of the alluvial plain extending downdip with increasing rates of RSL fall, forming a series of broad erosional surfaces and distributing deposition fairly evenly across the width of the alluvial plain. These broad surfaces produced a relatively planar erosional unconformity (sequence boundary) but no true incised valley. As noted in "Experimental Methods" the slow cycle was designed, by using a cycle length much greater than basin equilibrium time, to erode uniformly across the width of the basin. In contrast, during both the isolated and superimposed rapid cycles, a well defined incised valley formed. For all of these valleys, the fluvial system became progressively less incised downdip. As a result of this, topographic-valley depth also decreased downdip, such that near shore, valley incision diminished to the point where the fluvial delta did not incise (Fig. 5B, solid line with filled circles). This change from an incised to a non-incised system was accompanied by a rapid widening of the fluvial floodplain as it passed from being confined by valley walls to being unconfined and free to expand over the entire width of the experimental basin. Overhead video images of the experimental surface evolving during falling and rising GSL are available as supplementary material from the JSR data archive (see Acknowledgments section).

The explanation for this downdip change in valley depth is two-fold. First, because of decreasing rates of subsidence in the updip direction (Equation 2), during GSL fall, rates of RSL fall increased updip. This tended to increase the vertical depth of fluvial incision updip from shoreline. The second cause of the downstream decrease in topographic valley depth was that with rapid upstream valley incision, the downstream end of the valley tended to fill with sediment eroded upstream. Figure 6B illustrates the extent to which valley erosion (both valley incision and widening) contributed to overall deposition in the basin. In the experiment this downstream deposition during sea-level fall accelerated widening of the valley downstream, producing the trumpet-shaped valley planform observed. This shape is comparable to that found in many natural estuaries, and we see no reason why the causal mechanism (enhanced widening by downstream deposition) would not act at field scales as well.

It is important to note that while it is tempting to think of valley formation as being caused by a continuous process of excavation, in fact both the processes of deposition and erosion were occurring simultaneously, along the length of the valley. Valley formation results from an overall preponderance of erosion over deposition. For example, much of valley incision in the experiment resulted from the upstream migration of fluvial scours that formed a series of erosional steps (as defined by Sun and Parker 2005 and Taki and Parker 2005), visible as upstream-migrating standing waves in overhead videos taken during the experiment. These structures caused a considerable amount of downdip deposition, even though the overall effect was fluvial incision. We stress, however, that any form of highly localized erosion, such as knickpoint migration, can overload the system and produce localized deposition downstream.

Stratigraphic-Valley Depth

In general, downdip trends in stratigraphic-valley depth are opposite to downdip trends in topographic-valley depth. In Figure 5C stratigraphic-

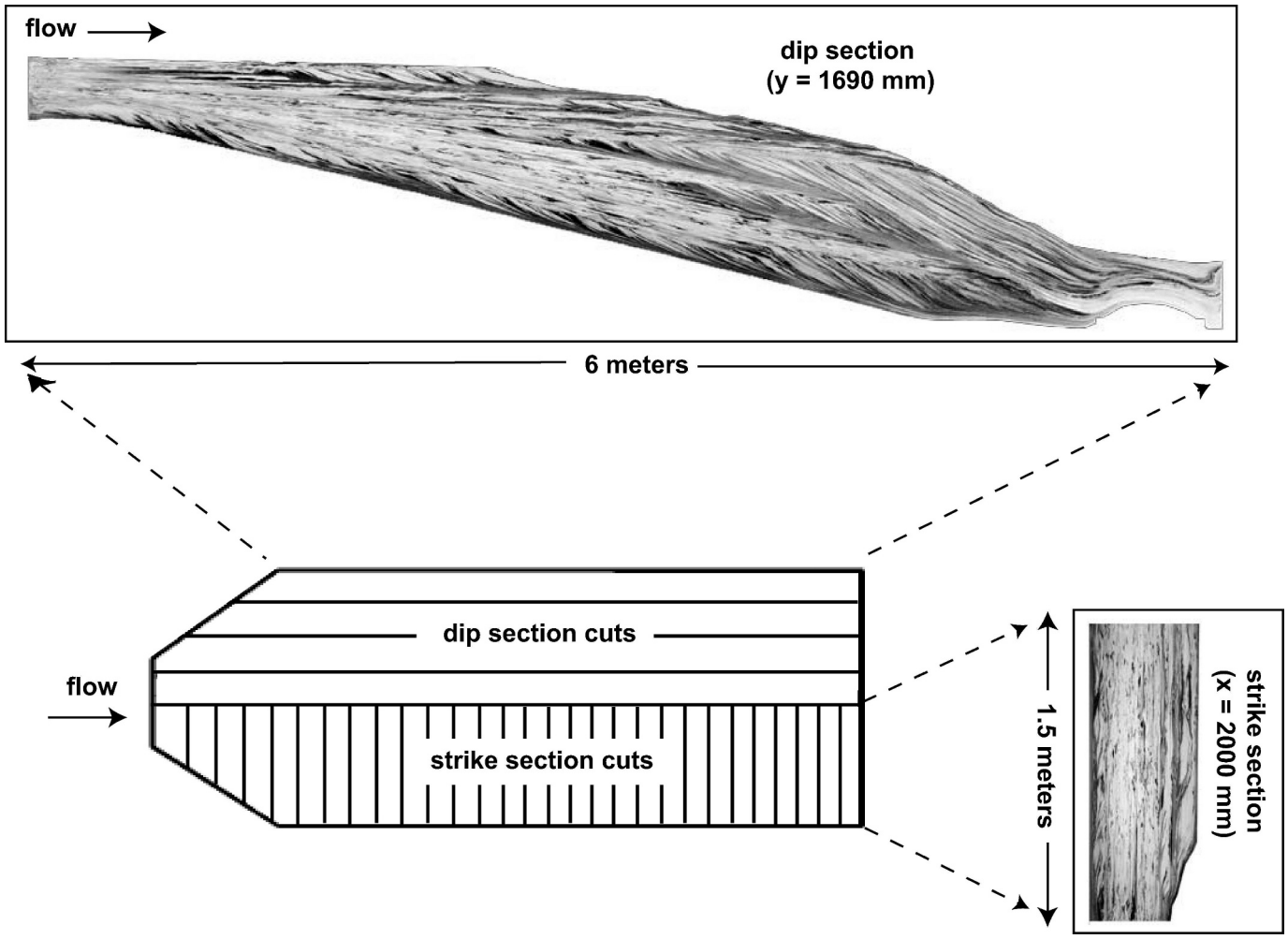

FIG. 4.—XES basin dip and strike section slicing scheme for Run 02.

incised-valley depth (plain solid line in Fig. 5C) increases downdip to about $x = 2000$ mm, and then decreases farther downdip to about 3000 mm, beyond which no incised-valley features exist. Also, even though during the experiment the incised-valley system (solid line with filled circles in Fig. 5B) extended to the updip-most part of the basin ($x = 0$ mm), there is little evidence of an incised valley in the experimental stratigraphy updip of about $x = 1500$ mm (solid line with filled squares in Fig. 5A, C, D). High resolution images of the experimental stratigraphy in dip and strike section, as well as movies of the evolution of the reconstructed experimental stratigraphy in dip and strike section are available as supplementary material from the JSR data archive (see Acknowledgments section).

There are two reasons for the downdip increase in stratigraphic-valley depth between 1500 mm and 2000 mm. First, the magnitude of GSL fall during the falling limb of the superimposed cycles was greater than that of the isolated rapid GSL fall (Fig. 2B). Therefore not all of the stratigraphic valley that formed during the isolated rapid GSL cycle was preserved. The extent to which the pre-existing isolated rapid-cycle stratigraphy was eroded during GSL fall increased updip, in concert with increasing rates of RSL fall during the first, second, and third superimposed sea-level cycles. This also explains why the updip limit of the stratigraphic valley is 1500 mm. Updip of $x = 1500$ mm the stratigraphic valley was completely eroded during falling sea level in subsequent GSL cycles. The second part of the explanation for the reversal in the sense of increase of valley depth between the topographic and stratigraphic valleys (Fig. 5B–D) is that the tendency of deposition to fill in the downdip part of the topographic valley does not influence the depth of the stratigraphic valley, which like any erosional surface is controlled only by the depth of the deepest scour to have occurred in that location.

As for why stratigraphic-valley depth then decreases from a maximum valley depth at $x = 2000$ mm to minimal to no valley visible at $x = 3000$ mm (Fig. 5B–D), the explanation is also two-fold. First, for this GSL cycle, $x = 2000$ mm is approximately the downdip limit of postdepositional erosion. Thus all strata downdip of about $x = 2000$ mm are not truncated by subsequent GSL cycles, such that for any given downdip location, preserved stratigraphic-valley depth $\approx$ maximum topographic-valley depth (Fig. 5D). Second, since we are restricting our discussion in this paper to subaerial valley incision, during the experiment shoreline position demarcated the maximum possible downdip location at which an incised valley could have formed, and in that way controlled the valley depth. In other words, during the experiment, downdip of the active shoreline, valley depth was zero. Furthermore, valley depth was also dependent on how long a given location had been exposed subaerially and had experienced RSL fall (Eq. 1). Therefore, downdip of $x \approx 2500$ mm (highstand shoreline) the rate at which the topographic valley depth decreased, and ultimately the rate at which the stratigraphic-valley depth decreased, downstream

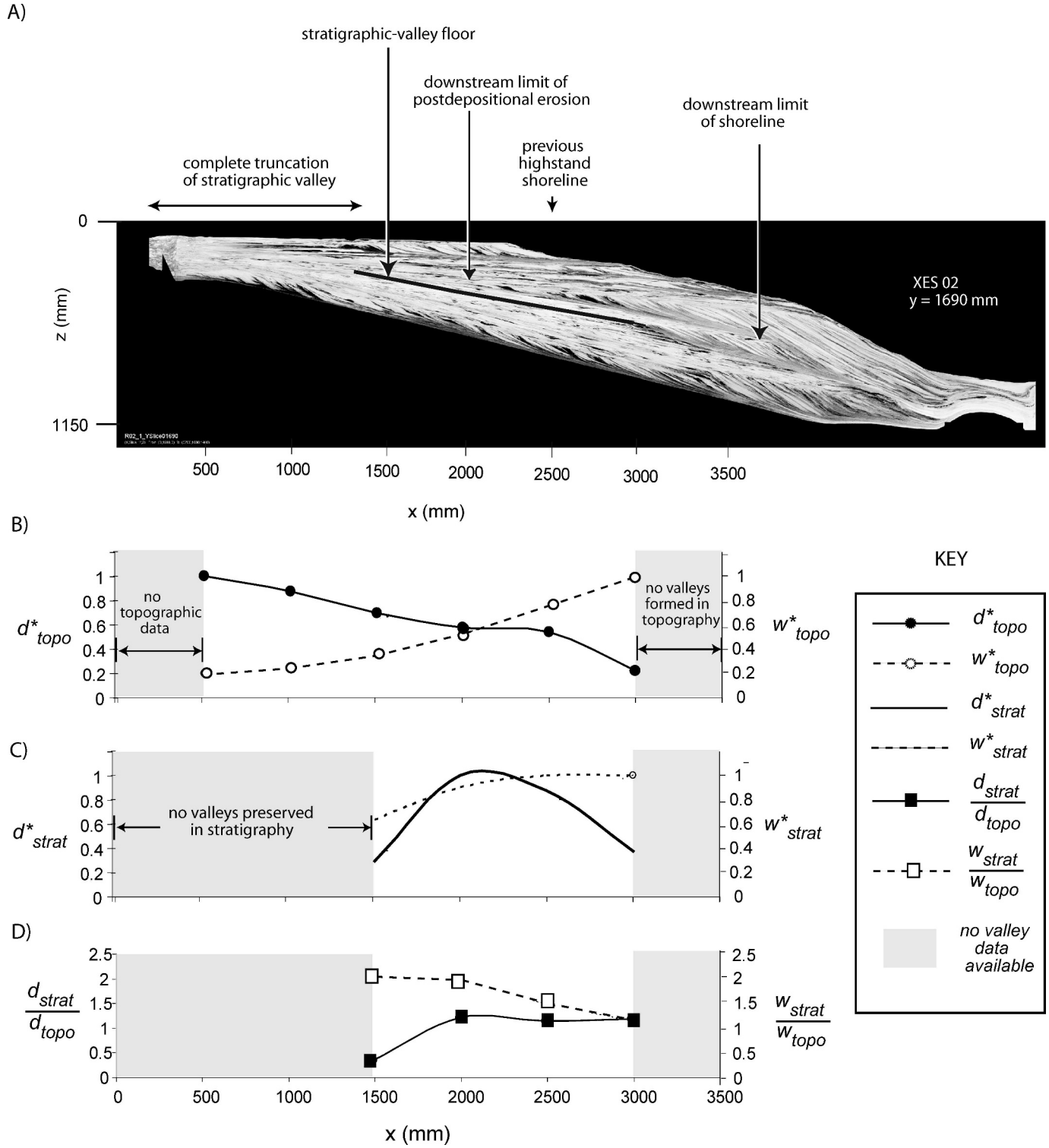

FIG. 5.—**A)** The experimental deposit in dip section. This is an actaul image of the stratigraphy as it looked at the end of the run. The basement of the deposit is slanted due to the subsidence geometry. Flow in the experiment was from left to right. All comments such as "complete truncation of stratigraphic valley," "stratigraphic-valley floor," etc., refer to stratigraphy and events related to the isolated rapid eustatic cycle. Note that the *x* axes of Figure 6A, B, C, and D are all aligned with one another, so that all information in one graph correlates spatially with the other two. **B)** Downdip change in topographic-valley width and depth are illustrated by the help of two nondimendional numbers: (1) nondimensional topographic-valley width, w^*_{topo} (the ratio of topographic-valley width for a given downsteam location, *x*, to the maximum topographic-valley width (dashed line with open circles)), and (2) nondimensional topographic-valley depth, d^*_{topo} (the ratio of topographic-valley depth for a given downsteam location, *x*, to the maximum topographic-valley depth (solid line with filled circles)). **C)** Downdip changes in stratigraphic width and depth are illustrated by the help of two nondimendional numbers: (1) nondimensional stratigraphic valley width, w^*_{strat} (the ratio of stratigraphic-valley width for a given downsteam location, *x*, to the maximum stratigraphic-valley width (plain dashed line)), and (2) nondimensional stratigraphic-valley depth, d^*_{strat} (the ratio of stratigraphic-valley depth for a

(Fig. 5B, C) was a function not only of downdip changes in subsidence rates but also of the rate at which the shoreline prograded during the fall. Finally, at the end of the fall, the shoreline had migrated to $x \approx 3600$ mm (Fig. 5A), yet the topographic valley extended downdip only to about $x = 3000$ mm (Fig. 5B). The reason that the downstream limit of the valley is approximately 600 mm upstream of the downstream limit of shoreline is that there is a minimal amount of localized erosion that must occur in order to restrict fluvial incision to an incised valley and prevent it from migrating across the entire basin width. We find that the minimal amount of local erosion needed to restrict fluvial incision to initiate valley formation is a depth that is greater than one bankfull channel depth (the autogenic scour depth) and that this minimal amount of incision must occur in a time scale that's short relative to the time it takes for the channel to avulse to a new location. For this experiment the average autogenic scour depth was ~ 20 mm and the minimal amount of local erosion needed to restrict fluvial incision to initiate valley formation was about twice the average autogenic scour depth (~ 40 mm).

Topographic-Valley Width

For all of the GSL cycles, valley width was influenced by two competing processes: narrowing during incisional events and widening associated with erosion of valley walls. As noted in Strong and Paola (2006), by enhancing lateral channel mobility, deposition tends to accelerate valley widening. In addition, autogenic processes of channel incision, deposition, and migration act to localize and randomize the incision and widening process. The general trend is of valley incisional narrowing during accelerating RSL fall and deposition and widening during both decelerating RSL fall and during RSL rise. Hence, the minimum valley width and the maximum rate of basinward shoreline migration coincide with the maximum rate of fall, i.e., when

$$\left.\frac{\partial RSL}{\partial t}\right|_x < 0 \text{ and } \left.\frac{\partial^2 RSL}{\partial t^2}\right|_x = 0,$$

as apposed to at lowstand when

$$\left.\frac{\partial RSL}{\partial z}\right|_x < 0 \text{ and } \left.\frac{\partial^2 RSL}{\partial z^2}\right|_x = 0.$$

During the rapid GSL cycles, soon after GSL fall began, an incised valley began to form. The incised valley narrowed with increasing rates of RSL fall and then slightly widened as the rate of fall decreased towards the end of the fall. During RSL rise, valley widening continued throughout the entire rise. Figure 7 illustrates a simplified hypothetical example of valley width and depth evolution in response to changing rates of RSL fall and RSL rise. Figure 7 illustrates how the incised-valley unconformity changes shape and becomes progressively more amalgamated and time transgressive through time, even in this simplified two-dimensional scenario.

In the more complex and heterogeneous natural world the composite, time-transgressive nature of these unconformities could be even stronger. To get an idea of just how much more complicated patterns of erosion and deposition can be in natural systems, consider how wetted width (a temporally high-resolution proxy for valley width in the experiment) changed throughout the isolated rapid GSL cycle. Figure 6C illustrates how fractional wetted width, w^*_{wet}, changes throughout the isolated rapid GSL cycle, where $w^*_{wet} = w_{wet}/W$ and w_{wet} is the total width of the alluvial plain covered in water, and W is the width of the alluvial plain. The smaller w^*_{wet}, the greater the degree of channel incision, and vice versa. Figure 6C indicates that, while the fluvial system is on average incisional throughout most of the GSL fall and is on average depositional throughout most of the GSL rise, there is an interplay of erosion and deposition during the entire cycle. Incisional narrowing is followed by deposition and channel migration during GSL fall, and depositional widening is interrupted by frequent incision during GSL rise. All of this leads to the likelihood of (1) isolated deposition being preserved from the GSL fall stage and (2) valley-fill sediments being reworked and the basal erosional unconformity reshaped by localized scour events during GSL rise. We return to these observations in the Discussion section.

Stratigraphic-Valley Width

Although like topographic-valley width, stratigraphic-valley width increases downstream (dashed line in Fig. 5C), the stratigraphic valley is considerably wider than the topographic valley as it appeared in the landscape at the end of the isolated rapid GSL fall (dashed line with open squares in Fig. 5D). Valley filling coupled with valley widening during sea-level rise creates a stratigraphic valley that is wider and whose side slopes are considerably less than the side slopes of associated topographic valleys (Fig. 7G).

Diachrony of Stratigraphic Surfaces

As discussed in the Introduction, differences between topographic and preserved stratigraphic surfaces are associated with diachrony of the stratigraphic surfaces. Figure 8 shows maps of the age of the erosional unconformity associated with the isolated slow and rapid GSL cycles. To quantify the diachrony, we define a dimensionless time, samech, ס, as follows:

$$ס = 1 - t_{\max\_eros}/t_{tot} \quad (3)$$

where t_{max_eros} is the time into the GSL cycle at which the topographic elevation attains its minimum measured value (i.e., the time at which the erosion surface formed), and t_{tot} is the total duration of the GSL cycle. Figure 8 parts A and B were made by using topographic scans from the isolated slow and rapid GSL cycles, respectively, to determine the age (in terms of the number of hours into the cycle it was formed) of the basal erosional unconformity. The smaller the value of ס, the younger the unconformity. For example $ס = 0$ is the youngest age possible and signifies a surface that formed at the end of GSL rise, while $ס = 1$ is the oldest age possible and signifies a surface that formed at the beginning of GSL fall. The estimate of ס is limited by the time resolution of topographic scans (90 minutes for the rapid cycles), so that the diachrony shown in Figure 8 is an underestimate. Even with this limitation, the time maps show that these erosional unconformities, one associated with basin-wide erosion and the other associated with an incised-valley system, are highly time-transgressive surfaces.

Overall, the erosion surfaces associated with the isolated slow and rapid GSL cycles formed over a time range comparable to (or nearly equal to, in the case of the rapid cycle) the length of the whole cycle, as opposed to only during falling stage. Further, it is clear from these maps that, for

←

given downsteam location, x, to the maximum stratigraphic-valley depth (plain solid line)). **D)** Downdip changes in stratigraphic width, w_{strat}, relative to topographic width, w_{topo}, illustrated with the nondimensional number w_{strat}/w_{topo} (dashed line with open squares) and downdip changes in stratigraphic depth, d_{strat}, relative to topographic depth, d_{topo}, illustrated with the nondimensional number d_{strat}/d_{topo} (solid line with filled squares). Note that all topographic-valley widths and depths are for the topographic incised valley as it appeared in the landscape at the end of the isolated rapid eustatic fall.

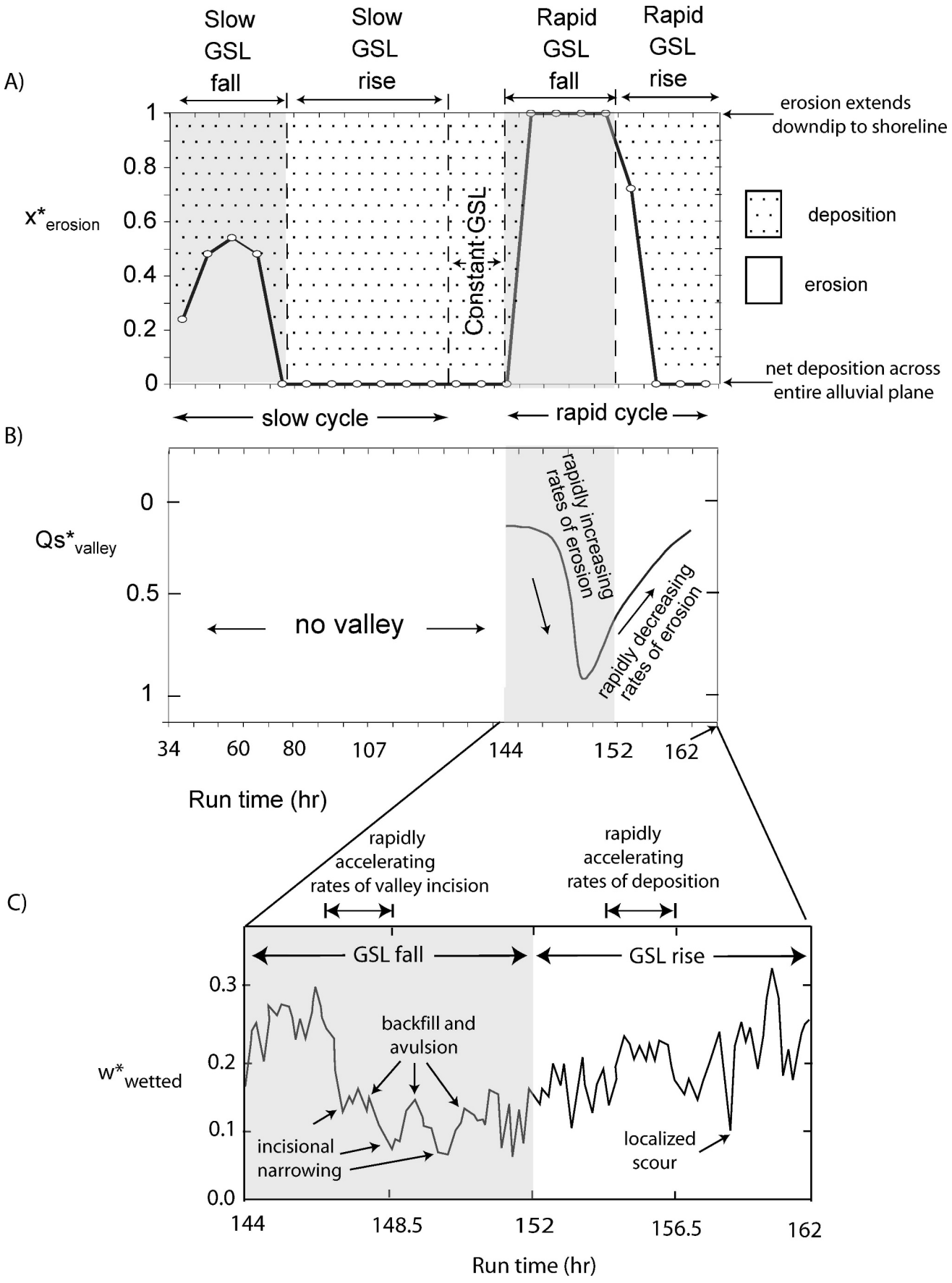
A)
Slow GSL fall
Slow GSL rise
Rapid GSL fall
Rapid GSL rise
erosion extends downdip to shoreline
x*erosion
Constant GSL
deposition
erosion
net deposition across entire alluvial plane
slow cycle
rapid cycle
B)
Qs*valley
rapidly increasing rates of erosion
rapidly decreasing rates of erosion
no valley
Run time (hr)
C)
rapidly accelerating rates of valley incision
rapidly accelerating rates of deposition
GSL fall
GSL rise
w*wetted
backfill and avulsion
incisional narrowing
localized scour
Run time (hr)

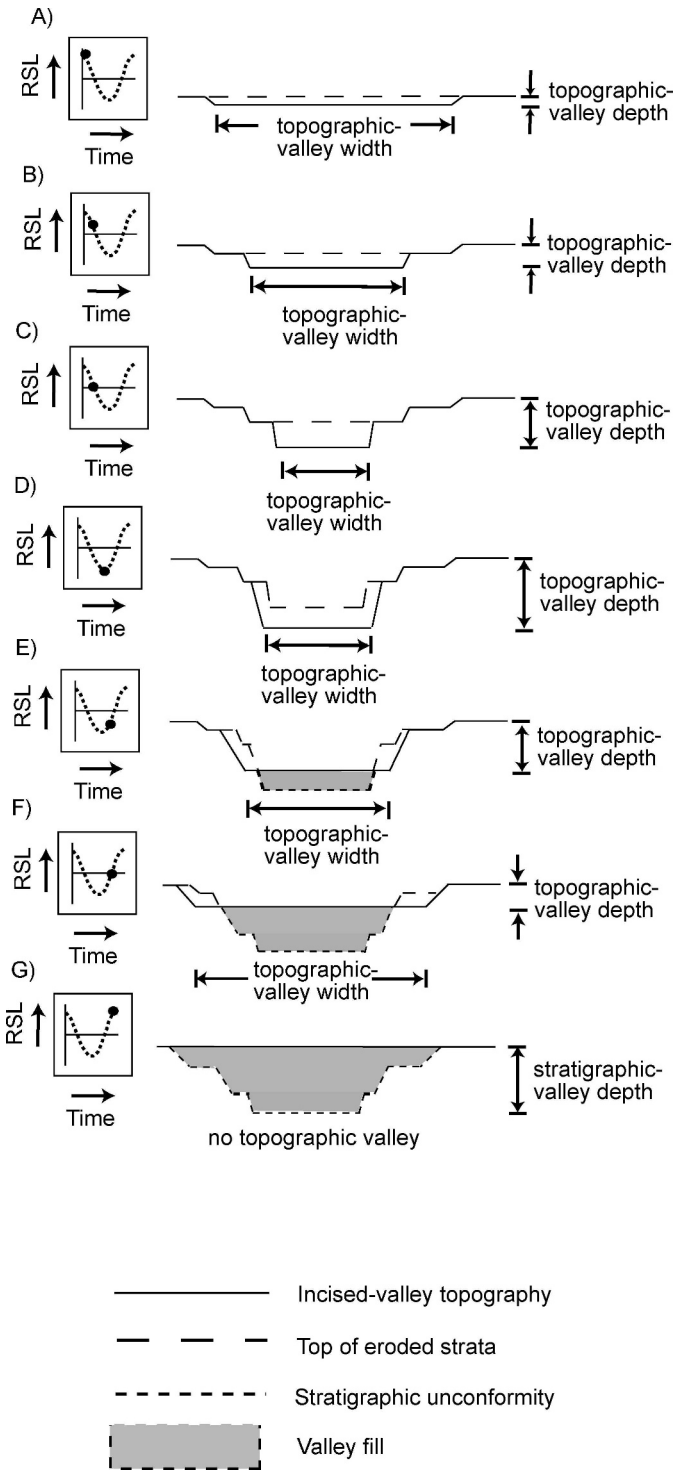

FIG. 7.—A simplified hypothetical model of valley width and depth evolution in response to changing rates of RSL fall and RSL rise (modified after Strong and Paola 2006).

both of these erosional surfaces, relative diachrony in dip section, although present, is significantly less than that in strike section. This reflects the importance of valley (depositional) widening during decelerating RSL fall and during RSL rise in creating the final stratigraphic valley (erosional unconformity). The dynamic evolution of valley width during the entire RSL cycle, coupled with autogenic variation in erosion and deposition, accounts for the diachronous nature of the valley system in strike section. Due to a combination of widening and aggradation during RSL rise, the youngest erosional events are generally preserved stratigraphically at the outer edges of the valley system at the end of the isolated rapid GSL cycle, while the oldest preserved erosional events are generally located at or near the valley axis.

Furthermore, for the isolated slow GSL cycle, incision began at the upstream-most part of the alluvial plain and not at the shoreline (Fig. 6A). The farther downdip, the later erosion began and the sooner it ended. As a result, at the end of the isolated slow GSL cycle, the oldest preserved erosional surfaces were (generally) farthest downdip and the youngest preserved erosional surfaces were (generally) farthest updip. In contrast, for the isolated rapid GSL cycle the entire incised-valley system was erosional during GSL fall, yet, like the slow GSL cycle, during GSL rise the downstream limit of erosion retrograded upstream with GSL rise. Thus, for both the slow and rapid isolated GSL cycles the stratigraphic valley is also time transgressive in dip section such that the age of the valley floor generally increases downdip.

Examples of exceptions to this general trend are clearly illustrated in the age maps of the basal erosional surface that formed during the slow and rapid eustatic cycles in Figure 8. Notice that in both maps that there are areas, albeit small in size, where the basal erosional surface is older than some of its downstream parts. Some of these older upstream and younger downstream sections are highlighted in the maps ($\eth = 1.0$ in Fig. 8A and $\eth = 0.75$ in Fig. 8B). Note also that the dashed line indicates the approximate location of shoreline at the time that these older erosional events occurred. Therefore at a time equivalent to $\eth = 1.0$ during the slow cycle or $\eth = 0.75$ during the rapid cycle, while these older erosional surfaces were forming, the sediments (foredelta deposits) that lie directly under the more downstream parts of the unconformity had not yet been deposited (shoreline had not yet prograded that far out onto the basin). Since these older erosional surfaces formed during localized deep scour events that quickly backfilled with deposition during subsequent channel migration (avulsion), sediments lying directly above these older sections of the unconformity are (within the resolution of our measurements) of the same age as the basal erosional surface and thus must be older in age than sediments lying directly below the surface in its more downstream sections. The sketch in Figure 9 illustrates how this process occurred in the experiment and how it could occur in a natural system as well.

It is important to note that the experimental design was such as to minimize the potential for downstream diachrony while maximizing that for lateral diachrony. Erosion due to upstream-migrating erosional steps (analogous to knickpoints) was rapid, because of the unconsolidated nature of the sediment mix; for our purposes it is effectively instantaneous. At the same time, the use of noncohesive sediment maximized the potential for valley-wall erosion and lateral diachrony. Finally, due to the coarse time resolution of the experimental topography scans (1.5–8 hr), the experimental design also minimizes estimates of

←

FIG. 6.—**A)** Changes in the erosional fraction of the alluvial plain, $x^*_{erosion}$, for the isolated slow and rapid GSL cycles, where $x^*_{erosion} = (x_{erosion}/x_{shoreline})$ where $x^*_{erosion}$ is the width-averaged downstream limit of erosion and $x^*_{shoreline}$ is the width averaged downstream position of shoreline. **B)** Changes in the fraction of sediment supply from valley erosion, Qs^*_{valley}, where Qs^*_{valley} = (volume of valley erosion/volume of deposition on the alluvial plain). **C)** Changes in fractional wetted width, w^*_{wetted}, for the isolated rapid cycle, where w^*_{wetted} = (width of the alluvial plane covered in water/total width of the alluvial plain). Note that Parts A, B, and C are all a function of time and that the time axis on Parts A and B is not isometric.

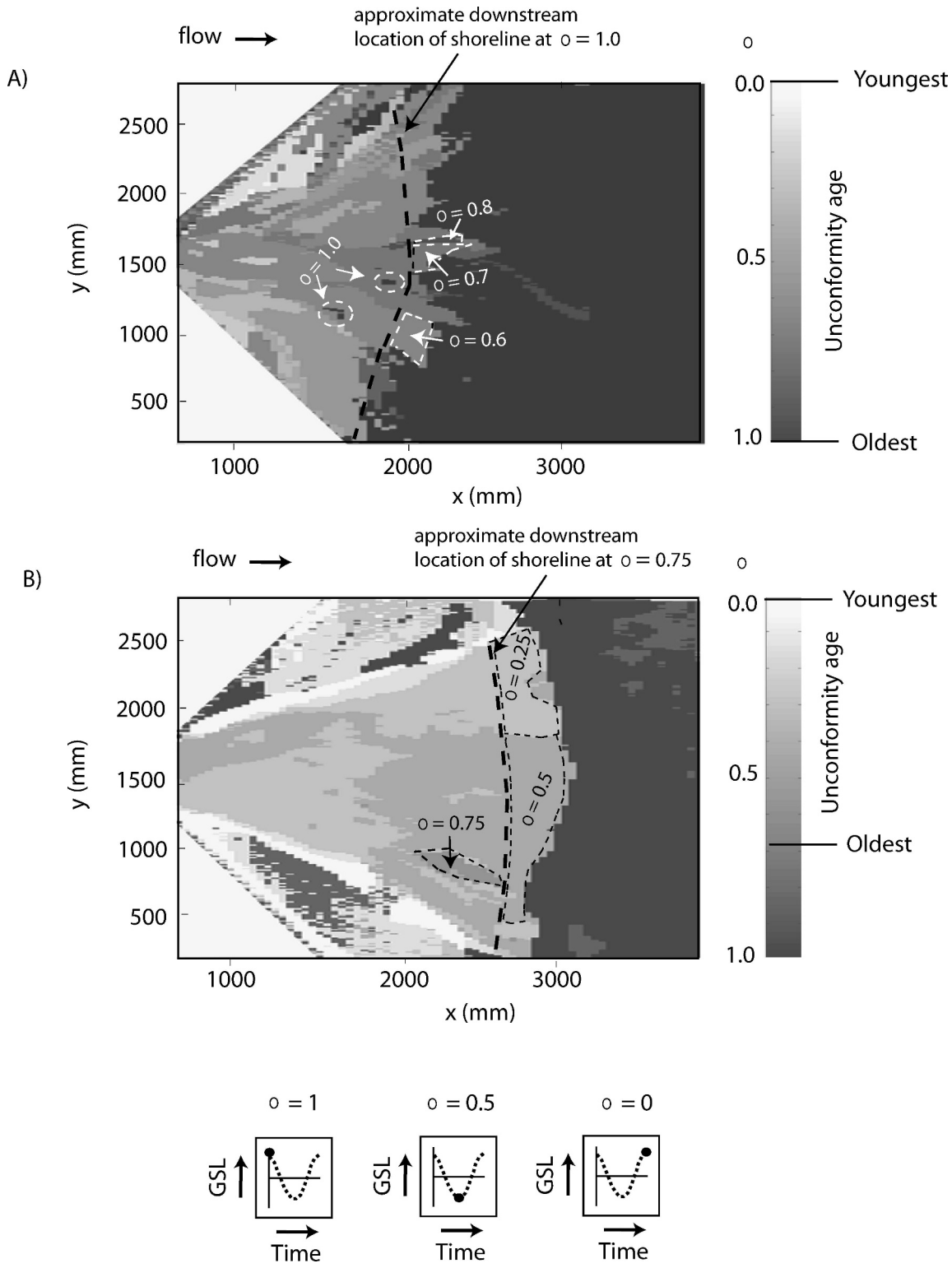

FIG. 8.—2D maps of the age of the basal erosional surface (unconformity) associated with the isolated **A)** slow and **B)** rapid GSL cycles. Samech, ϑ, is equal to the age of the basal erosional surface (in terms of the number of hours into the cycle it was formed) divided by the total number of hours in the cycle.

diachrony in general. More frequent topography scans would have allowed us to measure diachrony in the age of stratigraphic surfaces at a time resolution less than 90 minutes and thus provided a better resolved picture of the actual diachrony.

DISCUSSION

In terms of the general association between incised-valley formation and filling and base-level change, our experiment confirms concepts that

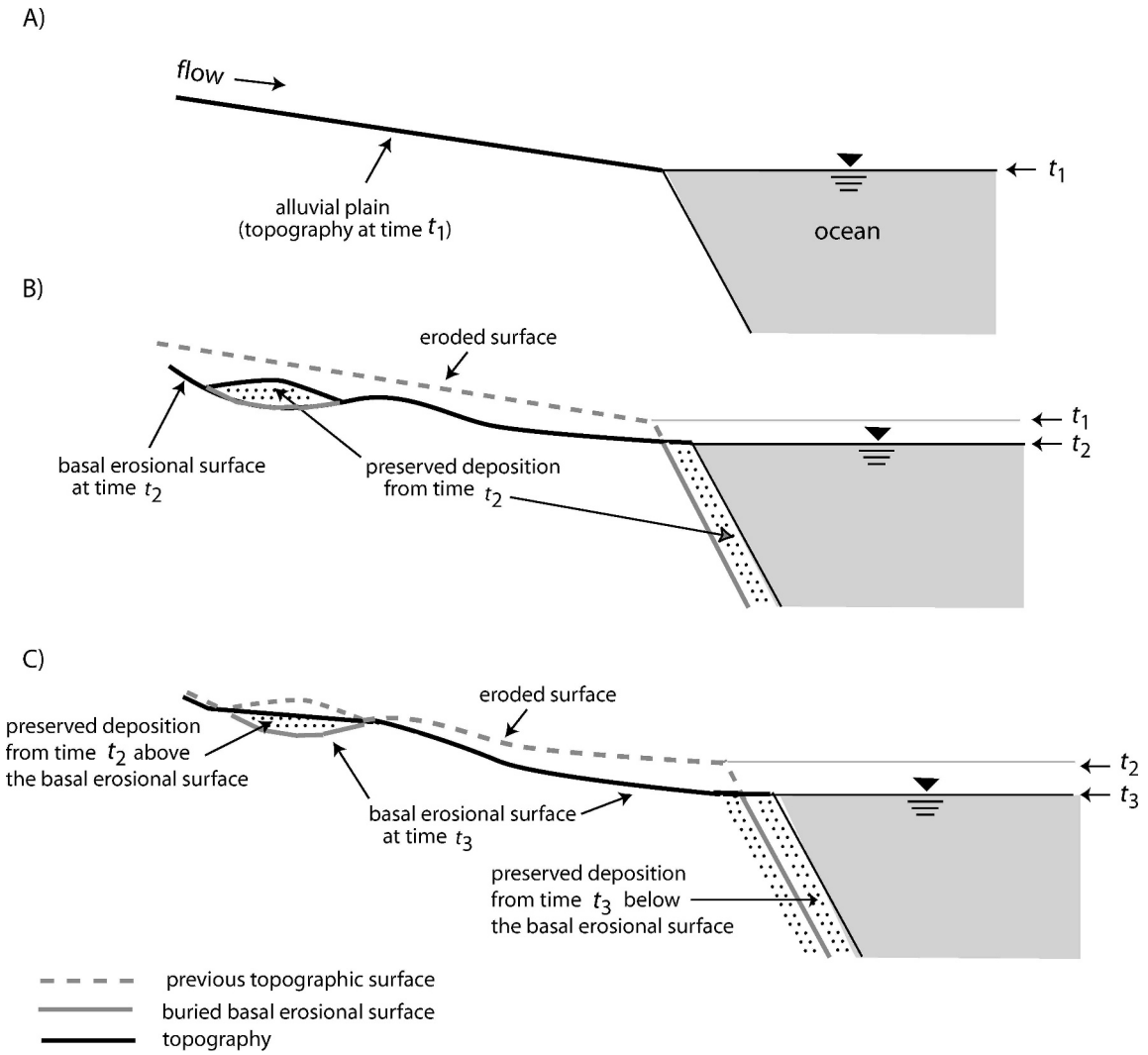

FIG. 9.—Schematic sketch illustrating how during the evolution of a basal erosional surface (unconformity) during RSL fall it is possible to preserve deposits above the basal erosional surface that are older than some of the deposits below it. **A)** Topographic surface (thick solid black line) before initial eustatic fall (gray dashed line in Parts B and C), **B)** location of basal erosional surface (thick solid black line) and preserved deposits (areas filled with speckled pattern) on the alluvial plain and delta foresets at the end of the initial eustatic fall at time t_2, and **C)** location of basal erosional surface and preserved deposits on the alluvial plain (from time t_2) and delta foresets (from time t_3) at the end of the second eustatic fall at time t_3. Note that the preserved deposit on the alluvial plain from time t_2 sits above, while the younger delta foresets from time t_3 sit below, the basal erosional surface that formed at time t_3.

previous workers have developed based only on the final product preserved in the rock record (e.g., Catuneanu 1998; Törnqvist et al. 2003). First, we observe that in order for a valley system to form there is a critical rate of erosion that must occur. For this experiment that rate is one that forces localized incision that is greater than one scour depth of autogenic incision in a time scale that's short relative to the time it takes for the channel to avulse to a new location. Second, we find that based on physical stratigraphy alone, reconstructing any of the paleo-conditions prevalent during valley incision is difficult, if not impossible, without temporally well constrained and well preserved downdip sediment accumulations from that time period. The preserved stratigraphic valley does not represent any incised valley that ever existed in the landscape: what we see preserved in stratigraphy is not a topographic surface but a composite valley-form erosional surface. This surface was produced over nearly all of its associated GSL cycles by random scour events that were loosely organized to create net erosion during RSL fall and net deposition during RSL rise, and then clipped by erosional events that occurred in later GSL cycles. Although they are valley-form in shape, these stratigraphic valleys represent valleys that never were, i.e., their geomorphic form never existed in the fluvial landscape. The extent to which topographic incised valleys are reworked during the GSL cycle is made clear by the time map of incised valley erosion from the isolated rapid GSL cycle unconformity (Fig. 8B). In this case, barely any record of the GSL fall is preserved. Mostly what is recorded in stratigraphy is GSL rise. The stratigraphic valley was completely reshaped during the last half—the *rising* limb—of the seal-level cycle.

Third, the surface that defines the erosional unconformity carved out by the incised valley system is highly diachronous both in dip and strike section. There may be cases in which assigning chronostratigraphic significance to an incised valley surface is a useful heuristic, but fundamentally these surfaces are not timelines. In the experimental deposit, basal erosional unconformities spanned as much as an entire sea-level cycle in terms of age (Fig. 8). Fourth, during RSL fall valleys form through a continuous process of channel incision, deposition, and migration (Fig. 6C). Therefore, during RSL fall there are areas in the basin that cut and then backfill. After backfilling, erosion shifts laterally.

Eventually, the fluvial erosion surface may reoccupy an abandoned and partly filled old channel, but portions of these older channel fills are still preserved above the amalgamated fluvial erosional surface. Ultimately, old fluvial valley fills lie on top of an extended erosion surface that overrides younger delta fronts. The net result is that the erosional unconformity is a highly diachronous, amalgamated surface that does not satisfy a commonly quoted characteristic of a sequence boundary, namely that it separates everywhere older from everywhere younger rocks.

CONCLUSIONS

1. The large-scale incisional stratigraphic valleys created by base-level cycles evolve dynamically over most of the base-level cycle, including the rise.
2. Incised valleys as preserved stratigraphically tend to be most diachronous along lateral margins of valley fill in proximal areas of the basin and become somewhat younger on average landward along their axial parts. Because they are continually reshaped during the base-level cycle, they are composite features that represent neither a specific topographic surface nor a specific time.
3. Stochastic erosion and deposition during incised-valley evolution lead to numerous, though relatively small-scale, deviations from one of the frequently quoted fundamental characteristics of a sequence boundary, which is that rocks above it are everywhere younger than rocks below it.
4. Slow RSL fall leads to a broad flat erosion surface (“slow” as defined relative to the basin theoretical “equilibrium time” of Paola et al. 1992). Rapid RSL fall leads to river incision and narrowing of the active floodplain, creating an incised-valley system. In order for a valley system to form there is a critical rate of erosion that must occur. For this experiment that rate is one that allows localized incision that is at least twice the autogenic incision depth in a time scale that’s short relative to the time it takes for the channel to avulse to a new location.
5. Fluvial systems became progressively less incised and floodplains widened downdip, both because subsidence increased basinward and because river incision increased sediment supply to areas downstream.
6. The characteristic mode of valley evolution changes throughout a period of RSL fall and rise. Valleys deepen and narrow with increasing rates of RSL fall, deepen and widen during decelerating RSL fall, and then fill and continue to widen during RSL rise. Valleys are narrowest during the period of most rapidly accelerating RSL fall (most rapid regression).
7. Erosional unconformities associated with incised-valley systems are wider and have shallower sidewall slopes than any of the topographic valleys they record. They also tend to shallow downstream, while in the stratigraphic record they appear in general to deepen downstream. The mismatch between stratigraphic (preserved) and topographic (instantaneous) valley geometry is associated with systematic diachrony in the preserved valleys.

ACKNOWLEDGMENTS

The authors would like to thank Jim Mullin, Chris Ellis, Dick Christopher, Ben Sheets, Wonsuck Kim, John Swenson, Tom Hickson, Dan Cazanacli, Lincoln Pratson, and numerous others unmentioned for help with the enormous task of running these experiments. The authors would also like to thank Paul Myrow, Becky Dorsey, Collin North, Brian Willis, John Southard, Charlie Winker, and Janok Bhattacharya for discussions and suggestions that helped shape and greatly improve the manuscript. Finally, we would like to thank our sponsors, the National Center for Earth-surface Dynamics (NCED), a Science and Technology Center funded by the Office of Integrative Activities of the National Science Foundation (under agreement Number EAR- 0120914) and the St. Anthony Falls Industrial Consortium (Anadarko, ChevronTexaco, ConocoPhillips, ExxonMobil, Japan Oil, Gas and Metals Corporation). The data described in this article are available from the JSR data archive, URL: http://www.sepm.org/jsr/jsr_data_archive.asp.

REFERENCES

Ashley, G.M., and Sheridan, R.E., 1994, Depositional model for valley-fills on a passive continental margin, *in* Dalrymple, R.W., Boyd, R.J., and Zaitlin, B.A., eds., Incised-Valley Systems: Origin and Sedimentary Sequences: SEPM, Special Publication 51, p. 285–301.

Blum, M.D., and Price, D.M., 1998, Quaternary alluvial plain construction in response to glacio-eustatic and climatic controls, Texas Gulf Coastal Plain, *in* Shanley, K.W., and McCabe, P.J., eds., Relative Role of Eustasy, Climate, and Tectonism in Continental Rocks: SEPM, Special Publication 59, p. 31–48.

Blum, M.D., and Törnqvist, T.E., 2000, Fluvial response to climate and sea-level change: a review and look forward: Sedimentology, v. 47 (Supplement), p. 1–48.

Bromely, M.H., 1991, Architectural features of the Kayenta Formation (Lower Triassic), Colorado Plateau, USA: relationship to salt tectonics in the Paradox Basin: Sedimentary Geology, v. 73, p. 77–99.

Brookfield, M.E., 1977, The origin of bounding surfaces in ancient eolian sandstones: Sedimentology, v. 24, p. 303–332.

Catuneanu, O., Willis, A., and Miall, A.D., 1998, Temporal significance of sequence boundaries: Sedimentary Geology, v. 121, p. 157–178.

Dalrymple, M., 2001, Fluvial reservoir architecture in the Statfjord Formation (northern North Sea) augmented by outcrop analogue statistics: Petroleum Geoscience, v. 72, p. 115–122.

Ethridge, F.G., Germanoski, D., Schumm, S.A., and Wood, L.J., 2005, The morphological and stratigraphic effects of base-level change: a review of experimental studies, *in* Blum, M., Marriott, S., and Leclair, S., eds., Fluvial Sedimentology VII: International Association of Sedimentologists, Special Publication, p. 213–241.

Heller, P.L., Paola, C., Hwang, I., John, B., and Steel, R., 2001, Geomorphology and sequence stratigraphy due to slow and rapid base-level changes in an experimental subsiding basin (XES 96-1): American Association of Petroleum Geologists, Bulletin, v. 85, p. 817–838.

Kim, W., Paola, C., Voller, V.R., and Swenson, J.B., 2006, Experimental measurement of the relative importance of controls on shoreline migration: Journal of Sedimentary Research, v. 76, p. 270–283.

Kraus, M.J., and Middleton, L.T., 1987, Dissected paleotopography and base-level changes in a Triassic fluvial sequence: Geology, v. 15, p. 18–21.

Lopez-Gomez, J., and Arche, A., 1993, Architecture of the Canizar fluvial sheet sandstones, Early Triassic, Iberian Ranges, eastern Spain, *in* Marzo, M., and Puigdefabregas, C., eds., Alluvial Sedimentation, International Association of Sedimentologists, Special publication 17, p. 363–381.

Nemec, W., and Steel, R.J., 1984, Alluvial and coastal conglomerates: their significant features and some comments on gravelly mass-flow deposits, *in* Koster, E.H., and Steel, R.J., eds., Sedimentology of Gravels and Conglomerates, Canadian Society of Petroleum Geologists, Memoir 10, p. 1–31.

Paola, C., Heller, P.L., and Angevine, C.L., 1992, The large-scale dynamics of grain-size variation in alluvial basins, 1: Theory: Basin Research, v. 4, p. 73–90.

Paola, C., Mullin, J., Ellis, C., Mohrig, D.C., Swenson, J.B., Parker, G., Hickson, T., Heller, P.L., Pratson, L., Syvitski, J., Sheets, B., and Strong, N., 2001, Experimental stratigraphy: GSA Today, v. 117, p. 4–9.

Posamentier, H.W., and Allen, G.P., 1999, Siliciclastic sequence stratigraphy: concepts and applications: SEPM, Concepts in Sedimentology and Paleontology, no. 7, 210 p.

Rubin, D.M., 1987, Cross-Bedding, Bedforms, and Paleocurrents: SEPM, Concepts in Sedimentology and Paleontology, 187 p.

Schumm, S., 1977, The Fluvial System: New York, John Wiley & Sons, 338 p.

Shanley, K.W., and McCabe, P.J., 1993, Alluvial architecture in a sequence stratigraphic framework: a case history from the Upper Cretaceous of southern Utah, USA, *in* Flint, S.S., and Bryant, I.D., eds., The Geological Modelling of Hydrocarbon Reservoirs and Outcrop Analogues, International Association of Sedimentology, Special Publication 15, p. 21–55.

Shanley, K.W., and McCabe, P.J., 1994, Perspectives on the sequence stratigraphy of continental strata: American Association of Petroleum Geologists, Bulletin, v. 78, p. 544–568.

Shanley, K.W., and McCabe, P.J., 1998, Relative role of eustasy, climate, and tectonism in continental rocks: an introduction, *in* Shanley, K.W., and McCabe, P.J., eds., Relative Role of Eustasy, Climate, and Tectonism in Continental Rocks: SEPM, Special Publication 59, p. iii–iv.

Sheets, B.A., Hickson, T.A., and Paola, C., 2002, Assembling the stratigraphic record: depositional patterns and time-scales in an experimental alluvial basin: Basin Research, v. 14, p. 287–301.

Sheets, B.A., Paola, C., and Kelberer, J.M., 2008, Creation and preservation of channel-form sand bodies in an experimental alluvial system, *in* Nichols, G., Williams, E., and Paola, C., eds., Sedimentary Processes, Environments and Basins: A Tribute to Peter Friend, International Association of Sedimentologists, Special Publication 38, p. 555–567.

Strong, N., 2006, Mass balance effects in clastic fluvial stratigraphy [Ph.D. Thesis]: University of Minnesota, Minneapolis, Minnesota, 126 p.

Strong, N., and Paola, C., 2006, Fluvial landscapes and stratigraphy in a flume: The Sedimentary Record, v. 4, no. 2, p. 4–7.

Strong, N., Sheets, B.A., Hickson, T.A., and Paola, C., 2005, A mass-balance framework for quantifying downstream changes in fluvial architecture, *in* Blum, M., Marriott, S., and Leclair, S., eds., Fluvial Sedimentology VII, International Association of Sedimentologists, Special Publication 35, p. 243–253.

Sun, T., and Parker, G., 2005, Transportational cyclic steps created by flow over an erodible bed: Part 2. Theory and numerical simulation: Journal of Hydraulic Research, v. 43, p. 502–514.

Taki, K., and Parker, G., 2005, Transportational cyclic steps created by flow over an erodible bed. Part 1. Experiment: Journal of Hydraulic Research, v. 43, p. 488–501.

Törnqvist, T.E., Wallinga, J., and Busschers, F.S., 2003, Timing of the last sequence boundary in a fluvial setting near the highstand shoreline—insights from optical dating: Geology, v. 31, p. 279–282.

Van Heijst, M.W.I.M., and Postma, G., 2001, Fluvial response to sea-level changes: a quantitative analogue, experimental approach: Basin Research, v. 13, p. 269–292.

Van Heijst, M.W.I.M., Postma, G., Meijer, X.D., Snow, J.N., and Anderson, J.B., 2001, Quantitative analogue flume-model study of river-shelf systems: principles and verification exemplified by the late Quaternary Colorado River-delta evolution: Basin Research, v. 13, p. 243–268.

Van Wagoner, J.C., Posamentier, H.W., Mitchum, R.M., Vail, P.R., Sarg, J.F., Loutit, T.S., and Hardenbol, J., 1988, An overview of sequence stratigraphy and key definitions, *in* Wilgus, C.K., Hastings, B.S., Kendall, C.G.St.C., Posamentier, H.W., Ross, C.A., and Van Wagoner, J.C., eds., Sea-Level Changes: An Integrated Approach: SEPM, Special Publication 42, p. 39–45.

Van Wagoner, J.C., Mitchum Jr., R.M., Campion, K.M., and Rahmanian, V.D., 1990, Siliciclastic Sequence Stratigraphy in Well Logs, Core, and Outcrops: Concepts for High-Resolution Correlation of Time and Facies: American Association of Petroleum Geologists, Methods in Exploration Series no. 7, 55 p.

Weissmann, G.S., Mount, J.F., and Fogg, G.E., 2002, Glacially driven cycles in accumulation space and sequence stratigraphy of a stream-dominated alluvial fan, San Joaquin Valley, California, U.S.A.: Journal of Sedimentary Research, v. 72, p. 240–251.

Received 18 August 2007; accepted 6 February 2008.